

Characterization of nanofiltration membranes with uncharged solutes

Z. Kovács*, W. Samhaber

*Institut für Verfahrenstechnik, Johannes Kepler Universität Linz,
Welser Straße 42, A-4060 Leonding, Austria.*

Abstract

The transportation of non-charged solutes through nanofiltration (NF) membranes is usually characterized by the term of molecular weight cut-off (MWCO) that is in the range of about 200-1500 Dalton. However, there are currently no standard methods for characterizing and reporting MWCO. The meaning of this information can vary between different membrane manufactures, and the applied experimental technique has a significant impact on the measured MWCO value. In this study, the separation performances of five commercial NF and tight ultrafiltration membranes (DK, GE, GH, NP030, NP010) were investigated using experimental permeation data of six noncharged solutes with various molecular weights. The membranes were characterized with their hypothetical pore sizes and their MWCO values were determined using two types of steric pore flow models, the steric-hindrance-pore (SHP) and the Donnan-steric-pore (DSP) model. Thermodynamical analysis of the experimental data was performed in order to obtain the reflection coefficients of the solutes, and the obtained phenomenological parameters were then linked to the membrane structural parameters. The overall best-fitting pore size radii in a least-squares sense were computed for each membrane by fitting to the sets of experimental data of reflection coefficients and solute radii. The predictions of both DSP and SHP models were found to be in a good agreement with the experimental data. However, a significant difference was found in the estimated pore size values depending on which measure of the solute size was employed and depending on the applied models. The provided values of membrane pore size can be used to predict the rejection of any noncharged solute for a given applied pressure.

Key words: nanofiltration, steric hindrance pore model, Spiegler-Kedem, uncharged, molecular weight cut-off

* Corresponding author.

Email address: zoltan.kovacs@jku.at (Z. Kovács).

1 Introduction

Nanofiltration (NF) membranes are a relatively recent development in the field of pressure-driven membrane separations, and their properties lie between ultrafiltration (UF) and reverse osmosis (RO). Due to its potential advantages, NF has gained a strong market position, brought about a number of patents, industrial research projects and commercial installations [1]. Starting in the late sixties, NF membrane processes have gradually found their way into industrial applications in various fields such as water softening, dye recovery, treatment of metal contained waste waters, oil-water separation, demineralization of whey, recycle of nutrients in fermentation processes, purification of landfill leachate, removal of sulfates from sea-water, bioproduct separation [2].

NF systems are usually operated at medium pressures in the range of 10-50 bar, and have much higher water fluxes compared to RO membranes. NF can be applied for separation between ions with different valences and for separation of low- and high-molecular weight components. Polymeric NF membranes show diversity in separation behaviour but they are common in rejecting highly charged ions (such as SO_4^{2-} , CO_3^{2-} , PO_4^{3-} , Mg^{2+}) in a higher degree, while in comparison, rejection of single charge ions (Cl^- , Na^+ , K^+) is much less. NF also rejects uncharged, dissolved material and positively charged ions according to the size and shape of the molecule in question [3].

The transportation of non-charged solutes through an NF membrane is usually characterized by the term of molecular weight cut-off (MWCO), which is a number expressed in Dalton indicating the molecular weight of a hypothetical non-charged solute that is in 90% rejected. The MWCO of NF membranes is usually given by the manufacturers and typically in the range of about 200-1500 Dalton. However, there are currently no standard methods for characterizing and reporting MWCO. The meaning of this information can vary between different membrane manufactures, thus limiting its value. The applied experimental technique has a significant impact on the measured MWCO. The experimental conditions, such as the hydrodynamic flow conditions, the temperature, the applied pressure or the range of the applied pressure-scan, the type of solute(s), are often not reported. Besides, the different techniques for MWCO make membranes from different manufacturers hardly comparable without further experimental investigations. Moreover, the concept of MWCO does not address the question of how great the permeation of solutes smaller and larger than the indicated MWCO can be.

Membranes have been historically characterized by MWCO rather than by membrane pore size [4]. It should be noted that this concept is based on practical aspects and has no true physical meaning. The molecular weight is not a straightforward measure of the size and it ignores the shape of the permeating

molecule, and thus, it gives only a rough estimation of the membrane's ability to remove dissolved uncharged components.

The term *nanofiltration* was introduced by the membrane manufacturer FilmTec highlighting that such membranes are capable to retain uncharged molecules with the size of about 1 nm, and which corresponded well with the early predictions of Sourirajan and Matsuura about the membranes' hypothetical capillary pore size [5]. However, it is still the subject of scientific debates whether NF membranes can be considered as porous or nonporous media.

Several direct characterization methods are known for NF membranes such as permoporometry, gas adsorption-desorption and microscopy techniques. However, the pore size determination of polymeric membranes seems to be still an unsolved problem. Permporometry analysis requires pores larger than 2 nm [6], and the nitrogen adsorption-desorption method only for inorganic membranes can be effectively applied. As far as microscopy is concerned, Bowen et al. [7] analysed the structural parameters of NF membranes with atomic force microscopy (AFM) and claimed that AFM images provide direct confirmation of the presence of discrete pores of nanometre dimensions in such membranes. However, the authors reported that AFM can only give information of the surface pore dimensions as the tip cannot probe into the depth of the pore. Singh et al. [8] also pointed out that an important requirement for AFM pore size determination is a very low surface roughness, hence it is difficult to distinguish between the pores and the depressions in the membrane surface.

Models that adequately describe the separation behaviour of membranes are important since these are needed in the design of NF processes. NF is a complex process lying between UF and RO, thus models from both these areas and their combinations can be used to describe NF performance. These models rely on fundamentally different concepts and can be divided into the following types: irreversible thermodynamics models, nonporous or homogenous models, and pore models.

The properties of dry membranes are subject to changes in the presence of water. Thus, during the filtration, a swollen polymeric network is obtained which likely does not contain discrete pores. [5] In contrary to polymers, the morphology of inorganic membranes does not change by contacting with water. Well established characterization methods prove that inorganic NF membranes contain discrete pores in the order of 0.5 to 2 nm. Despite this morphological difference, both type of membranes show very similar separation behaviours, and their performance can be predicted with the same models assuming hypothetical pores in the near- or sub-nanometre range. However, in the pore models, the terms 'pore' or 'capillary' refer to any connecting polymer material-free void space through which fluid transport can take place under a

driving force [9].

In this paper we investigate the separation behaviour of NF membranes using experimental permeation data of six noncharged solutes. We use an indirect characterization method employing two types of steric pore flow models which are described in Sect.2.2, and we discuss possible concepts for solute size determination in Sect.2.3. We characterize five NF and tight UF membranes with their hypothetical pore sizes and determine their MWCO values with the different models.

2 Theory

2.1 Spiegler–Kedem model

The Spiegler–Kedem model (SK) [10] is based on the principles of irreversible thermodynamics and has found a wide use for the description of RO and NF membrane separations. This phenomenological approach treats the membrane as a black box, and no insight is given into the membrane structure and morphology. The relation between the rejection \mathcal{R} and the solvent volume flux J_v is given by the expression:

$$\mathcal{R} = \frac{\sigma \left(1 - \exp \left(\frac{\sigma - 1}{P_s} J_v \right) \right)}{1 - \sigma \exp \left(\frac{\sigma - 1}{P_s} J_v \right)}, \quad (1)$$

where the two membrane parameters are the reflection coefficient σ and the solute permeability coefficient P_s .

The rejection is defined as

$$\mathcal{R} = 1 - c_p/c_r, \quad (2)$$

where c_p and c_r represent, respectively, the solute concentrations in the permeate and retentate streams.

2.2 Models of hindered transport

The modelling of solute transport through the membrane is based on the extended Nernst–Planck equation accounting for diffusion, convection and electromigration. For uncharged species, when electrostatic effects are negligible, the transport equation for the molar solute flux j_s is given as the sum of the diffusive and the convective terms as follows

$$j_s = K_c c V - D_p \frac{dc}{dx}, \quad (3)$$

where V is the solvent velocity, K_c is the convective hindrance factor and D_p is the hindered solute diffusivity in the membrane pores. This latter is given as the product of the bulk diffusivity D_∞ and the diffusive hindrance factor K_d , and corrected with the factor η_0/η_p which accounts for the solvent pore viscosity η_p versus the bulk viscosity η_0 . There it holds:

$$D_p = K_d D_\infty \frac{\eta_0}{\eta_p}. \quad (4)$$

The Donnan-steric-pore-model (DSP) was originally developed by Bowen et al. [7]. They have introduced the following relationships between the ratio of solute to pore radius λ and the hindrance factors K_c and K_d :

$$K_c = (2 - \Phi) (1 + 0.054\lambda - 0.988\lambda^2 + 0.441\lambda^3), \quad (5)$$

$$K_d = 1 - 2.30\lambda + 1.154\lambda^2 + 0.224\lambda^3, \quad (6)$$

where the steric partitioning coefficient Φ (neglecting concentration polarisation) is given as

$$\Phi = (1 - \lambda)^2. \quad (7)$$

The model assumes a fully developed solute velocity inside the pores and assumes a Hagen-Poiseuille type parabolic profile. The solvent velocity in cylindrical pores with constant circular cross-sections can be obtained from the Hagen-Poiseuille law:

$$V = \frac{r_p^2 (\Delta P - \Delta\pi)}{8\eta_p (\Delta x/A_k)} \quad (8)$$

where x/A_k is the ratio of effective membrane thickness to membrane porosity, η_p is the solvent viscosity in the pore, ΔP is the applied pressure, and $\Delta\pi$ is the osmotic pressure difference across the pore.

The bulk solvent properties can significantly differ from the properties of thin liquid layers present in narrow pores. In a recent study of Bowen et al. [11], the ratio of bulk solvent viscosity η_0 and pore viscosity η_p was expressed as a function of pore size r_p in the following form:

$$\frac{\eta_p}{\eta_0} = 1 + 18(d/r_p) - 9(d/r_p)^2, \quad (9)$$

where d is the thickness of oriented solvent layer.

Eq.(8) can be introduced into Eq(3), and since the solute flux can be rewritten as $j_s = c_p V$, the integration of the concentration gradient across the membrane thickness yields:

$$\mathcal{R} = 1 - \frac{K_c \Phi}{1 - (1 - K_c \Phi) \exp(-Pe_m)}, \quad (10)$$

where the modified dimensionless Peclet number Pe_m is defined as

$$Pe_m = \frac{K_c V \Delta x}{K_d D_p A_k}, \quad (11)$$

and indicates the relative importance of convection over diffusion.

Thus, Eq. (10) allows us to determine the limiting rejection:

$$\mathcal{R}_{lim} = 1 - K_c \Phi. \quad (12)$$

A similar approach to Bowen et al. [7] was used by Nakao et al. [12] to develop the steric-hindrance pore (SHP) model, which was later applied by Wang et al. [13] to predict the separation performance of NF membranes. In the SHP model, the phenomenological coefficient σ obtained from the Spiegler–Kedem analysis is linked to the membrane morphological parameter λ as follows:

$$\sigma = 1 - \left(1 + \frac{16}{9}\lambda^2\right) (1 - \lambda)^2 [2 - (1 - \lambda)^2] \quad (13)$$

Note that as far as neutral solutes are considered, Eq.(13) only differ from Eq.(12) in the analytical expressions for K_c and K_d described in Eqs. (5).

More detailed description of the SHP model can be found in other studies [12–14].

It should be pointed out that these models assume a spherical solute transport in parallel cylindrical membrane pores with identical and constant circular cross-sections. Pore size distribution is not considered in this paper.

2.3 Molecular size

Several measures of the molecular size are known such as the Stokes radius, the diameter derived from the hydrodynamic volume or from molar volume, the effective diameter, and the molecular width [15]. Among them, the effective diameter was found by Van der Bruggen et al. [16] to be the most suitable for describing filtration phenomena, as it reflects the projection of the molecule on the membrane. An empirical correlation between the effective radius r_E and the molecular weight Mw was determined as follows [15]:

$$r_E = 0.0325(Mw)^{0.438}. \quad (14)$$

The Stokes radius r_S for the uncharged molecules at a given molecular weight Mw can be determined by using the following empirical relation given by Bowan et al. [17]:

$$\log r_S = -1.4854 + 0.461 \log(Mw). \quad (15)$$

Finally, the relation between the diffusivity and molecular size can be calculated with the Stokes–Einstein equation:

$$D_\infty = \frac{kT}{6r_S\pi\eta}. \quad (16)$$

3 Experimental

Five commercial polymeric NF and tight UF membranes were employed in this study. The membrane specifications given by the manufacturers are shown in Table 1.

Chemicals of analytical degree used in the experiments were purchased from Sigma–Aldrich and Serva–Feinbiochemica. Their properties are shown in Table

Table 1
Membrane specifications given by the manufacturers

Name	DK	GE (G-5)	GH (G-10)	NP030	NP010
Manufacturer	GE W&P Technologies			Microdyn-Nadir	
Internet	http://www.geawater.com			http://www.microdyn-nadir.com	
Material of separation layer	proprietary			permanently hydrophilic PES	
Retention of uncharged solutes	150-300 ¹	1000 ²	2500 ²	70-90 ³	25-45 ³
Pure water flux [L/h/m ² /bar]	5.5 ± 25%	1.2 ± 25%	3.2 ± 25%	1-1.8	5-10
Classification	NF	UF	UF	NF	NF

¹ MWCO [Da] characterized on glucose and sucrose

² MWCO [Da] characterized on polyethylene glycol

³ Lactose rejecton [%] (test conditions: 4% solution, 40 bar, stirred cell (700 rpm), 20 °C)

Table 2
Molecular weights, effective and Stokes radii, and diffusivities of neutral solutes in aqueous solutions at 25 °C.

Solute	Mw [g/mol]	r_E ¹ [nm]	r_S ² [nm]	D_∞ ³ [$10^{-9}m^2/s$]
n-Butanol	74.1	0.21	0.24	1.03
D-Ribose	150.1	0.29	0.33	0.74
D-Glucose	180.2	0.32	0.36	0.68
D-Lactose Monohydrate	360.3	0.43	0.49	0.50
Polyethylene glycol	570-630	0.54	0.62	0.39
Dextran	≈ 900	0.64	0.75	0.33

¹ calculated with Eq.(14); ² calculated with Eq.(15); ³ calculated with Eq.(16)

3.

Membrane filtration was performed using the experimental set-up shown in Fig.1.

The membrane unit is equipped with a DDS LAB20 plate-and-frame module. Membrane discs with the effective membrane surface area of 350 cm² were placed in series and simultaneously tested. Single-component solutions of 100 ppm concentration were used. Both permeate and retentate streams were recycled into the feed tank. The cross-flow rate was set to 500 L/h which ensures a negligible concentration polarisation effect [18]. During the filtration experiments the applied trans-membrane pressure was changed between 0 and 40 bar. In all runs, stabilization time of 30 minutes was used before taking samples. Permeate flux was manually measured by using a calibrated cylinder

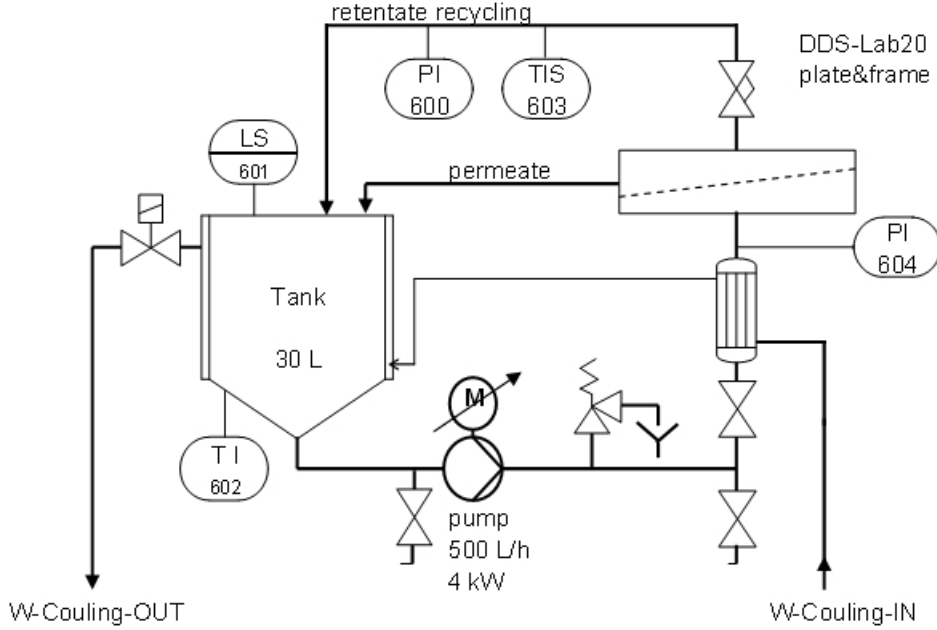


Fig. 1. Schematic diagram of the lab-scale membrane system

and a stopwatch. Concentrations of solutes were determined by total organic carbon analyzer (TOC 500, Shimadzu). All experiments were carried out at 25°C .

4 Results and discussion

The measured permeate fluxes versus applied pressure for the five membranes are shown in Fig.2. The slopes of the curves are equal to the hydraulic permeability of the respective membranes, which indicates that the osmotic pressure effects of the solutes are negligible due to the low feed concentrations.

For each sets of measured data of flux J_v and the rejection \mathcal{R} , Eq.(1) was used to compute the values of the membrane parameters σ and P_s with nonlinear two-parameter fitting in a least-squares sense. The σ corresponds to the maximum rejection at infinite volume flux. The results of the SK analysis are illustrated in Fig.3 using the permeation data of lactose as an example.

Prior to the steric pore model analysis, two main steps were performed. First, the reflection coefficients of the 6 solutes were determined for the 5 membranes using the SK model. Second, the Stokes radii r_S and the effective radii r_E of all solutes were calculated from Eq.(15) and Eq.(14), respectively. Thus, using the solute radius and the respective reflection coefficient allow us to determine the hypothetical pore size for each membrane. The DSP model using Eq.(10) or alternatively, the SHP model using Eq.(13) can be fitted to the

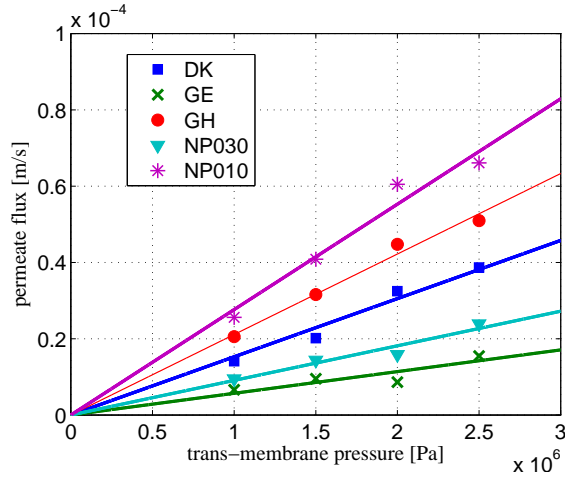


Fig. 2. Measured fluxes of lactose solution (symbols) and predicted fluxes based on pure water permeability (solid lines) for the 5 membranes.

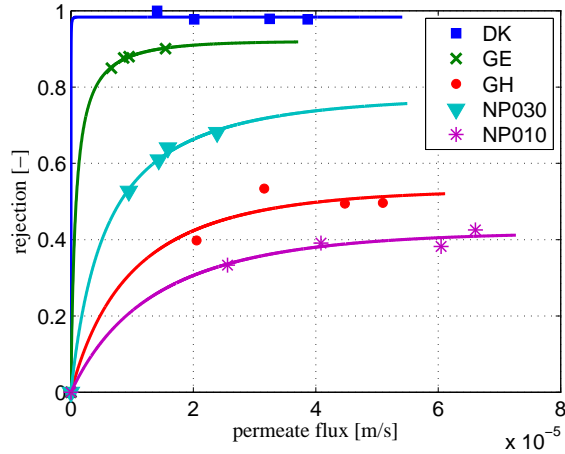


Fig. 3. Experimental data (symbols) of lactose rejection as function of flux for the 5 membranes. Solid lines were fitted using the SK model.

reflection coefficient of each uncharged solute individually in order to estimate the pore size. This would result in slightly different estimated pore size values for each solute and an average value could be calculated to characterize each membrane. Nevertheless, in this study, the reflection coefficients of all solutes were considered to compute the pore size of each membrane, which gives the overall best-fitting solution in a least-squares sense.

The predictions of the DSP and the SHP models compared with the experimental data are shown in Fig.4 and Fig.5, respectively. The quality of the fit can be described with the coefficient of determination R^2 defined as

$$R^2 = 1 - \frac{\sum_i (\sigma_i - \sigma_i^*)^2}{\sum_i (\sigma_i - \bar{\sigma})^2}, \quad (17)$$

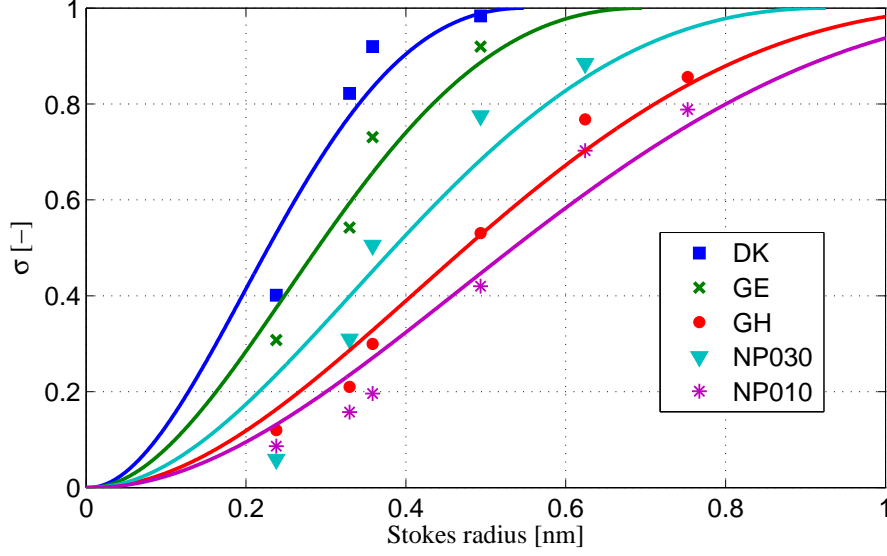


Fig. 4. Relationship between reflection coefficient (e.g. limiting rejection) and Stokes radii of solutes. The optimal estimates for the pore radii of the five membranes were provided from the model proposed by Bowen et al. using Eq(12). Solid lines illustrate model predictions with the best fitting r_p values.

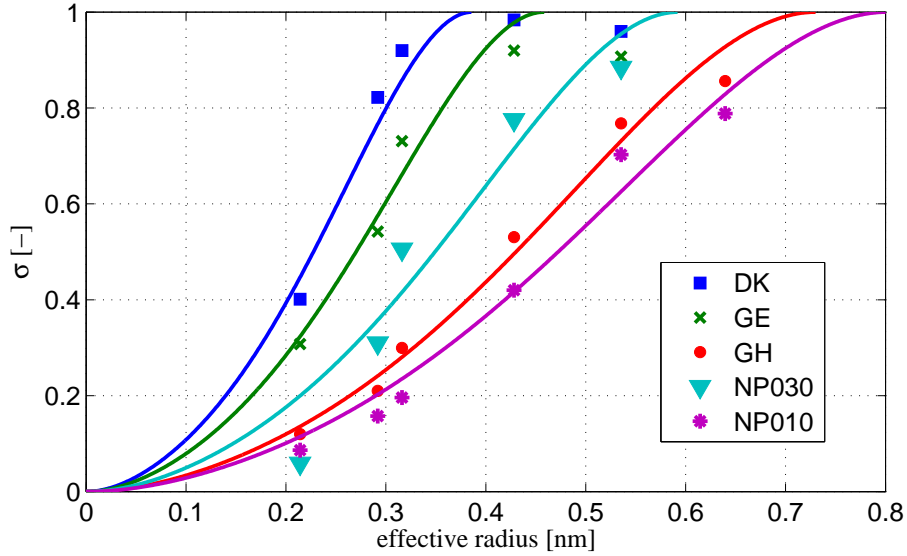


Fig. 5. Relationship between reflection coefficient (e.g. limiting rejection) and effective radii of solutes. The optimal estimates for the pore radii of the five membranes were provided from the SHP model using Eq(13). Solid lines illustrate model predictions with the best fitting r_p values.

where σ , σ^* and $\bar{\sigma}$ are the experimental, the modelled, and the mean of the experimental values, respectively. Using the determined pore sizes in the models allows us to compute the size of the molecule that has a limiting rejection of 90% and thus, the empirical relations described in Sect.2.3 can be used to

Table 3

Estimated hypothetical pore sizes of the five membranes obtained from SHP and DSP models using experimental data of neutral solutes.

membrane	SHP model						DSP model		
	using effective radius			using Stokes radius			using Stokes radius		
	rp[nm]	MWCO	R ²	rp[nm]	MWCO	R ²	rp[nm]	MWCO	R ²
GE	0.46	290	0.954	0.52	280	0.951	0.70	380	0.912
DK	0.39	200	0.940	0.44	200	0.925	0.55	230	0.807
GH	0.73	840	0.980	0.85	820	0.976	1.14	1100	0.923
NP030	0.59	520	0.915	0.68	500	0.917	0.93	700	0.934
NP010	0.80	1040	0.973	0.93	1010	0.976	1.29	1400	0.949

calculate the MWCO from the solute radius. The obtained data of r_p , MWCO and R^2 are listed in Table 4 for three different approaches. Overall, very good approximates of the measured data are given by both models. However, the pore sizes estimated by the DSP model are considerably bigger than the SHP model predictions. There is also a significant difference in the estimated pore size values depending on which measure of the solute size was employed in the SHP model.

The overall fittings of the studied two models are shown in Fig. 6 and Fig. 7. The estimated pore radii of the membranes listed in Table 4 and the Stokes radii as the measure of solute size were used to compute σ for each solute and for each membrane. Then, σ was plotted as a function of λ . As shown in Fig. 6 and Fig. 7, the experimental values of σ are in good agreement with the estimated σ values irrespective of which solute and membrane was applied.

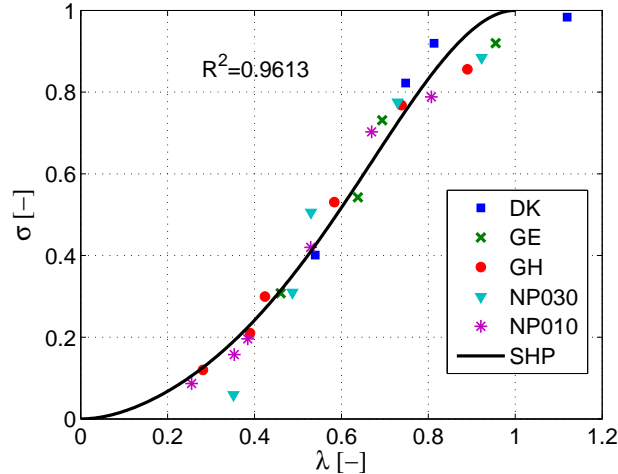


Fig. 6. Reflection coefficients of all solutes as a function of ratio of Stokes radii of the solutes to the pore radii of the five membranes. The curve was calculated from the SHP model with Eq.(13) using the pore radii r_p reported in Table 4.

It is important to note that combining Eq. 8, Eq. 10 and Eq. 11 provides a

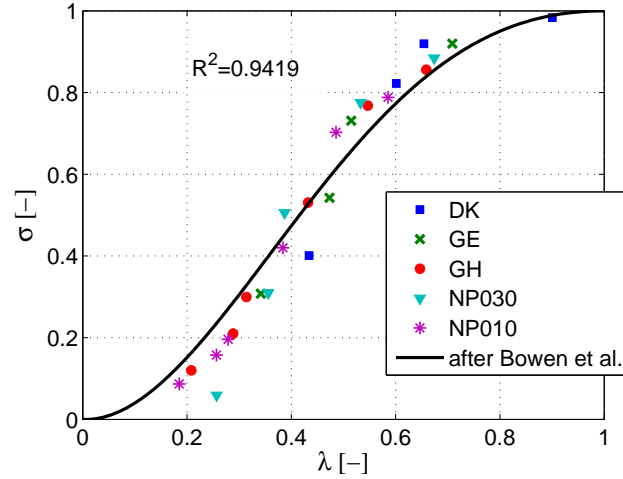


Fig. 7. Reflection coefficients of all solutes as a function of ratio of Stokes radii to the pore radii of the five membranes. The curve was calculated from the DSP model with Eq.(12) using the pore radii r_p reported in Table 4.

direct estimation of the pore size without the necessity of a prior SK analysis. The pore size can be obtained by fitting to the experimentally determined set of applied pressure and rejection data, or vice versa, the rejection of a noncharged solute for a given applied pressure can be calculated if the pore size of the membrane is known. This latter concept was applied to estimate the \mathcal{R} of the different solutes as a function of ΔP using the prior determined pore radius listed in Table 4. The model prediction is plotted together with the experimental data in Fig. 8 for the membrane GE as a representative membrane.

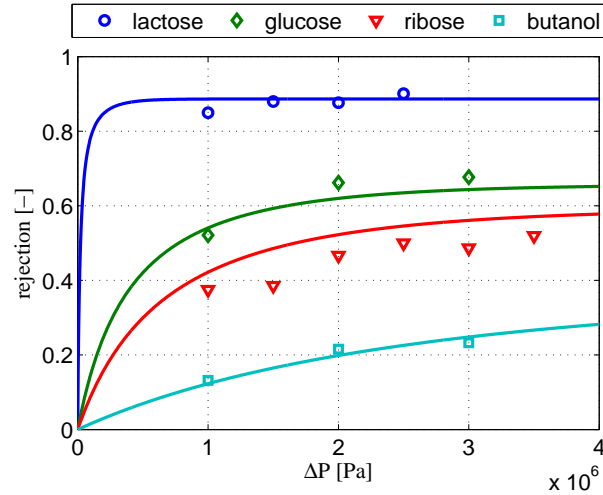


Fig. 8. Rejection of solutes as a function of permeate flux for the membrane GE. The curves were computed using Eq.(10) and assuming membrane pore radius $r_p = 0.70$ nm.

5 Conclusions

The hypothetical pore radii of five commercial NF membranes (DK, GE, GH, NP030, NP010) were evaluated from permeation experiments using different noncharged solutes. Thermodynamical analysis of experimental data was performed in order to obtain the reflection coefficients of each solute. This phenomenological parameter was linked to the membrane structural parameter using two steric pore flow models. The overall best-fitting solution in a least-squares sense was computed for each membrane by fitting the pore size radii to the sets of experimental data of reflection coefficients and solute radii. Predictions of both DSP and SHP models were found to be in a good agreement with the experimental data. However, there is a significant difference in the estimated pore size values depending on which model is used and also on which measure of the solute size is employed. The provided values of membrane pore size can be applied to predict the rejection of any noncharged solute for a given applied pressure.

References

- [1] D. Bessarabov, Z. Twardowski, Industrial application of nanofiltration - new perspectives, *Mem. Technol.* 9 (2002) 6–9.
- [2] J. Timmer, Properties of nanofiltration membranes: model development and industrial application, Ph.D. thesis, Technische Universiteit Eindhoven, Eindhoven, Netherlands (2001).
- [3] J. Wagner, *Membrane Filtration Handbook - Practical Tips and Hints*, Osmonics, Inc., Minnetonka USA, 2001.
- [4] S. Allgeier, *Membrane filtration guidance manual*, Tech. Rep. EPA 815-R-06-009, United States Environmental Protection Agency, Office of Water (2005).
- [5] A. Scafer, A. Fane, T. Waite, *Nanofiltration – Principles and Applications*, Elsevier Advanced Technology, Oxford UK, 2005.
- [6] F. P. Cuperus, D. Bargeman, C. A. Smolders, Permporometry: the determination of the size distribution of active pores in uf membranes, *J. Membr. Sci.* 71 (1992) 57–67.
- [7] W. Bowen, A. Mohammad, N. Hilal, Characterization of nanofiltration membranes for predictive purposes - use of salts, uncharged solutes and atomic force microscopy, *J. Membr. Sci.* 126 (1997) 91–105.
- [8] S. Singh, K. C. Khulbe, T. Matsuura, P. Ramamurthy, Membrane characterization by solute transport and atomic force microscopy, *J. Membr. Sci.* 142 (1998) 111–127.

- [9] K. Kosutic, L. Katelan-Kunst, B. Kunst, Porosity of some commercial reverse osmosis and nanofiltration polyamide thin-film composite membranes, *J. Mem. Sci.* 76 (168) (2000) 101–108.
- [10] K. Spiegler, O. Kedem, Thermodynamics of hyperfiltration (reverse osmosis): criteria for efficient membranes, *Desalination* 1 (1966) 311–326.
- [11] W. Bowen, J. Welfoot, Modelling the performance of membrane nanofiltration-critical assessment and model development, *Chem. Eng. Sci.* 57 (2002) 1121–1137.
- [12] S. Nakao, S. Kimura, Models of membrane transport phenomena and their applications for ultrafiltration data, *Chem. Eng. Japan* 15 (2) (1982) 200.
- [13] X. Wang, T. Tsuru, M. Togoh, S. Nakao, S. Kimura, Evaluation of pore structure pressure and electrical properties of nanofiltration membranes, *J. Chem. Eng. Jpn.* 28 (2) (1995) 186–192.
- [14] X. Wang, T. Tsuru, S. Nakao, S. Kimura, The electrostatic and steric-hindrance model for the transport of charged solutes through nanofiltration membranes, *J. Membr. Sci.* 135 (1997) 19–32.
- [15] B. V. der Bruggen, C. Vandecasteele, Modelling of the retention of uncharged molecules with nanofiltration, *Water Research* 36 (2002) 1360–1368.
- [16] B. V. der Bruggen, J. Shaep, D. Wilms, C. Vandecasteele, Influence of molecular size, polarity and charge on the retention of organic molecules by nanofiltration, *J. Mem. Sci.* 156 (1999) 29–41.
- [17] W. Bowen, A. Mohammad, Characterization and prediction of nanofiltration membrane performance - a general assessment, *Trans. IChemE* 76 (Part A) (1998) 885.
- [18] M. Teixeira, M. Rosa, M. Nystroem, The role of membrane charge on nanofiltration performance, *J. Membr. Sci.* 265 (2005) 160–166.

Table 4
Nomenclature

Symbol	Name	Unit
c_p	Permeate concentration	mol/m ³
c_r	Retentate concentration	mol/m ³
d	Thickness of oriented solvent layer	m
D_∞	Diffusion coefficient at infinite dilution	m ² /s
D_p	Hindered diffusion coefficient within the pore	m ² /s
j_s	Molar solute flux	mol/m ² /s
J_v	Volumetric permeate flux	m/s
k	Boltzmann constant ($1.38 \cdot 10^{-23}$)	J/K
K_c	Convective hindrance factor	–
K_d	Diffusive hindrance factor	–
Mw	Molecular weight	g/mol
Pe_m	Modified Peclet number	–
P_s	Solute permeability	m/s
\mathcal{R}	Rejection	–
\mathcal{R}_{lim}	Limiting rejection	–
r_E	Effective radius of solute	m
r_p	Pore radius	m
r_S	Stokes radius of solute	m
T	Temperature	K
V	Solvent velocity	m/s
x	Axial position within the pore	m
<i>Greek symbols</i>		
ΔP	Applied pressure	Pa
$\Delta \pi$	Osmotic pressure difference across the pore	Pa
Δx	Membrane thickness	m
Φ	Steric partitioning coefficient	–
η_0	Bulk dynamic viscosity	Pas
η_p	Dynamic viscosity within pores	Pas
λ	Ratio of solute to pore radius	–
σ	Reflection coefficient	–